– Supplemental material –
The adsorption height of epitaxial graphene: A criterion to assess the ideality of graphene?

J. Sforzini,[1,2] L. Nemec,[3] T. Denig,[4] B. Stadtmüller,[1,2] T-L. Lee,[5] C. Kumpf,[1,2] S. Subach,[1,2] U. Starke,[4] P. Rinke,[6,3] V. Blum,[7,3] F.C. Bocquet,[1,2,*] and F.S. Tautz[1,2]

[1]*Peter Grünberg Institut (PGI-3), Forschungszentrum Jülich, 52425 Jülich, Germany*
[2]*Jülich Aachen Research Alliance (JARA), Fundamentals of Future Information Technology, 52425 Jülich, Germany*
[3]*Fritz-Haber-Institut der Max-Planck-Gesellschaft, 14195 Berlin, Germany*
[4]*Max Plank Institute for Solid Research, Heisenbergstraße, 70569 Stuttgart, Germany*
[5]*Diamond Light Source Ltd, Didcot, OX11ODE, Oxfordshire, United Kingdom*
[6]*COMP/Department of Applied Physics, Aalto University, P.O. Box 11100, Aalto FI-00076, Finland*
[7]*Department of Mechanical Engineering and Material Science, Duke University, Durham, NC 27708 USA*

(Dated: November 10, 2014)

In the following, we discuss our measurements and calculations in more detail. In particular:

- Details on sample quality
- NIXSW details
- Influence of the DFT functional
- Bulk stacking order
- Influence of the polytype
- The electron density maps

DETAILS ON SAMPLE QUALITY

In order to check the quality of the QFMLG samples, we applied two different techniques. We first measured a low energy electron diffraction (LEED) pattern, a fast method to check the presence of long range order at the surface. A characteristic pattern is shown in Fig. 1. In addition, we performed angle resolved photoelectron spectroscopy, revealing the band structure of the surface. As shown in Fig. 2, the typical linear band dispersion expected for graphene is measured around the K-point of its surface Brillouin zone.

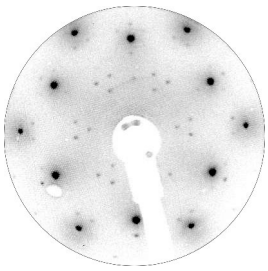

FIG. 1: LEED image taken with an incidence energy of 126 eV on QFMLG.

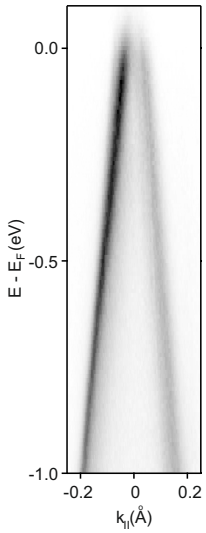

FIG. 2: ARPES spectrum of QFMLG performed in the ΓK direction and taken around K point (here at $k_{\parallel} = 0$) with the HeIα.

NIXSW DETAILS

The normal incidence x-ray standing wave technique gives access to adsorption heights of surface elements with respect to the lattice plane of a crystalline substrate. More details can be found in [1–3]. By tuning the incident photon energy (E) around the Bragg energy of the $H = (hkl)$ reflection, the spacial position of the x-ray standing wave field created in the vicinity of the surface shifts with respect to the lattice planes of the substrate. As a consequence, the photoelectron yield (Y) of a given adsorbed species varies. The resulting quantity, $Y(E)$, can be calculated with the following equation:

$$\begin{aligned} Y(E) =& 1 + S_R R \\ &+ 2F^H\sqrt{R}|S_I|\cos(\phi - 2\pi P^H + \Psi). \end{aligned} \quad (1)$$

By fitting the experimental data with eq. 1, two important independent parameters are extracted, for each

	P^H	F^H	d (Å)
Si_{Bulk}	0.019	1.23	0.048
C_{Bulk}	0.759	1.043	−0.607
$C_{Graphene}$	0.697	0.746	4.272

TABLE I: Averaged NIXSW measured values P^H and F^H for each component. The last column corresponds to the converted absolute positions with respect to the Bragg plane closest to the topmost Si atoms.

chemically differentiated species: the coherent position P^H and the coherent fraction F^H. P^H represents the average atomic positions and F^H can be understood as an order indicator of a given P^H. R and ϕ are the theoretical reflectivity and phase of the sample, respectively. The so-called non dipolar parameters, S_R, S_I and Ψ, were not used (that is to say set to 1, 1 and 0, respectively). The reason for this is that no reliable values are so far available for this geometry in the literature. All P^H and F^H values, averaged over all data sets, are shown in Tab. I. The value of both parameters should lie between 0 and 1. However non-dipolar effects [4] can influence the F^H values. This is clearly visible in the coherent fraction of silicon (1.23) for which a value very close to 1 is expected as it is a bulk species.

It is known that the graphene layer covers the steps of SiC(0001) [5], which as a consequence reduces the measured averaged coherent fraction (0.75), when compared to the perfectly flat C^{SiC}_{surf} (1.04). It is worth noting that for samples having a graphene coverage close but above one (not shown), the coherent fraction is dramatically reduced (0.48) in comparison to samples of coverage close but lower than one monolayer, measured on the same set-up (0.75).

Error bars estimation

Fitting the components of each core-level is rather simple as it requires a very simple fitting model and the peaks are well defined, Fig. 1(a,b) of the main article. The error bar of each component's area is determined by a Monte Carlo analysis and is much smaller than the symbols used in Fig. 1(c) of the main article. When fitting the electron yield, the P^H and F^H parameters of a given data set have a negligible error bar. However, when comparing data obtained from several spots on two different QFMLG samples, we observe small variations. We attribute this to possible sample inhomogeneities, or small beamline, manipulator and analyzer instabilities.

The values given in Tab. I are averaged over 7 C 1s and 2 Si2s data sets, as shown in Tab. II. For all species, the P^H varies by 0.022 at maximum. This corresponds to an error bar smaller than ±0.04 Å for absolute positions. For distances, the error is then ±0.06 Å.

Sample	Position	Species	P^H	F^H
A	1	Si_{Bulk}	0.020	1.229
A	2	Si_{Bulk}	0.018	1.230
A	3	C_{Bulk}	0.760	1.035
		$C_{Graphene}$	0.702	0.699
A	3	C_{Bulk}	0.760	1.041
		$C_{Graphene}$	0.698	0.788
A	1	C_{Bulk}	0.760	1.043
		$C_{Graphene}$	0.696	0.798
A	4	C_{Bulk}	0.760	1.041
		$C_{Graphene}$	0.707	0.580
A	5	C_{Bulk}	0.760	1.051
		$C_{Graphene}$	0.704	0.623
B	6	C_{Bulk}	0.758	1.048
		$C_{Graphene}$	0.688	0.864
B	7	C_{Bulk}	0.755	1.039
		$C_{Graphene}$	0.685	0.872

TABLE II: Coherent positions and fractions for each data set obtained on QFMLG.

INFLUENCE OF THE DFT FUNCTIONAL

The supplemental material of a previous work by some of the authors [6] included details on the numerical convergence of calculations for similar structures with respect to the number of basis functions and the grid density in real and reciprocal space. For the $(6\sqrt{3} \times 6\sqrt{3})$ interfaces we chose the Γ-point for accurate integrations in reciprocal space. The FHI-aims code employs numeric atom-centered basis sets. Basic descriptions of their mathematical form and properties are published in [7]. The basis set and numerical real space grids are of high quality as defined by the *tight* settings including a *tier*1+dg basis set for Si and a *tier*2 basis set for C [7].

To test the influence of the exchange correlation functional on the geometry we used three different exchange correlation functionals, the local density approximation (LDA) [8], the Perdew-Burke-Enzerhof generalized gradient approximation (PBE) [9] and the Heyd-Scuseria-Ernzerhof hybrid functional (HSE06)[10]. In HSE06 the amount of exact exchange is set to $\alpha = 0.25$ and a range-separation parameter $\omega = 0.2\text{Å}^{-1}$ is used.

For an accurate description of the different surface phases, in particular hydrogen-graphene bonding in the QFMLG phase, we include long range electron correlations, so-called van der Waals (vdW) effects. Here, we compare the results of two different schemes. The first scheme used in this work is the well established Tkatchenko-Scheffler (TS) [11] method. It is a pairwise approach, where the effective C6 dispersion coefficients are derived from the self-consistent electron density. The second approach is a more recent refinement to the TS scheme incorporating many-body effects [12–14]. In this scheme, the atoms are modelled as spherical quantum harmonic oscillators, which are coupled through dipole-dipole interactions. The cor-

6H-SiC ZLG															
	PBE+vdW			PBE+MBD			LDA			HSE06+vdW			HSE06+MBD		
n	$D_{n,n+1}$	d_n	δ_n Si/C	$D_{n,n+1}$	d_n	δ_n Si/C	$D_{n,n+1}$	d_n	δ_n Si/C	$D_{n,n+1}$	d_n	δ_n Si/C	$D_{n,n+1}$	d_n	δ_n
Z	2.37	—	—/ 0.30	2.35	—	—/ 0.29	2.30	—	—/ 0.37	2.38	—	—/ 0.30	2.37	—	—/ 0.30
1	1.92	0.48	$0.42/<10^{-2}$	1.92	0.51	$0.40/<10^{-2}$	1.91	0.53	$0.31/<10^{-2}$	1.92	0.48	$0.48/<10^{-2}$	1.92	0.48	$0.47/<10^{-2}$
2	1.88	0.61	$<10^{-2}/<10^{-2}$	1.89	0.61	$<10^{-2}/<10^{-2}$	1.88	0.60	$<10^{-2}/<10^{-2}$	1.88	0.61	$<10^{-2}/<10^{-2}$	1.88	0.61	$<10^{-2}/<10^{-2}$
3	1.89	0.62	$<10^{-2}/<10^{-2}$	1.90	0.63	$<10^{-2}/<10^{-2}$	1.88	0.62	$<10^{-2}/<10^{-2}$	1.88	0.62	$<10^{-2}/<10^{-2}$	1.89	0.62	$<10^{-2}/<10^{-2}$

6H-SiC QFMLG															
	PBE+vdW			PBE+MBD			LDA			HSE06+vdW			HSE06+MBD		
n	$D_{n,n+1}$	d_n	δ_n Si/C	$D_{n,n+1}$	d_n	δ_n Si/C	$D_{n,n+1}$	d_n	δ_n Si/C	$D_{n,n+1}$	d_n	δ_n Si/C	$D_{n,n+1}$	d_n	δ_n
G	2.75	—	$-/<10^{-2}$	2.76	—	$-/<10^{-2}$	2.71	—	$-/<10^{-2}$	2.71	—	$-/<10^{-2}$	2.77	—	$-/<10^{-2}$
H	1.50	—	—/—	1.50	—	—/—	1.51	—	—/—	1.49	—	—/—	1.49	—	—/—
1	1.89	0.62	$<10^{-2}/<10^{-2}$	1.89	0.62	$<10^{-2}/<10^{-2}$	1.88	0.61	$<10^{-2}/<10^{-2}$	1.88	0.62	$<10^{-2}/<10^{-2}$	1.88	0.61	$<10^{-2}/<10^{-2}$
2	1.89	0.63	$<10^{-2}/<10^{-2}$	1.89	0.63	$<10^{-2}/<10^{-2}$	1.88	0.63	$<10^{-2}/<10^{-2}$	1.88	0.63	$<10^{-2}/<10^{-2}$	1.88	0.63	$<10^{-2}/<10^{-2}$
3	1.89	0.63	$<10^{-2}/<10^{-2}$	1.89	0.63	$<10^{-2}/<10^{-2}$	1.88	0.62	$<10^{-2}/<10^{-2}$	1.88	0.62	$<10^{-2}/<10^{-2}$	1.88	0.63	$<10^{-2}/<10^{-2}$

TABLE III: Influence of the functional on the interface structure of 6H-SiC ($\sqrt{3}$-SiC model cell). $D_{n,n+1}$ is the distance between layer n and $n+1$, d_n gives the distance within SiC bilayer n, and δ_n the corrugation of layer n. All distances are given in Å.

responding many-body Hamiltonian is diagonalized to calculate the many-body vdW energies. As a result, this approach accounts for long-range many-body dispersion (MBD) effects employing a range-separated (rs) self-consistent screening (SCS) of polarizabilities and is therefore called MBD@rsSCS (for details see Ref. [14]). To include the long-range tail of dispersion interaction we couple each functional with either the pairwise TS scheme, here refered to as PBE+vdW (HSE06+vdW), or the MBD@rsSCS scheme in this work abbreviated as PBE+MBD (HSE06+MBD).

In Table III we list the layer distance ($D_{n,n+1}$), the Si-C distance within a SiC bilayer (d_n) and the layer corrugation (δ_n), the difference between the highest and lowest atom in the layer, for QFMLG and EMLG on 6H-SiC(0001) calculated with different exchange correlation functionals and vdW corrections. We conclude that PBE+vdW, PBE+MBD, HSE06+vdW and HSE06+MBD yield the same results for both phases.

BULK STACKING ORDER

For 3C-SiC(111), the stacking order close to the surface is independent of where the surface is cut. However, for the 6H-SiC(0001) this is different as the SiC bilayers are rotated every third layer by 30 degree in the unit cell. The position of the rotation is indicated in Fig. 3 by a kink in the grey line. We tested the influence of the stacking order for 6H-SiC using an approximated $\sqrt{3} \times \sqrt{3}$-R30° unit cell. The surface energies calculated using PBE+vdW of the 6H-SiC ZLG and the atomic structure are shown in Fig. 3. We find the lowest surface energy for ABCACB and ACBABC stacked SiC. We therefore use a ABCACB stacked 6H-SiC substrate.

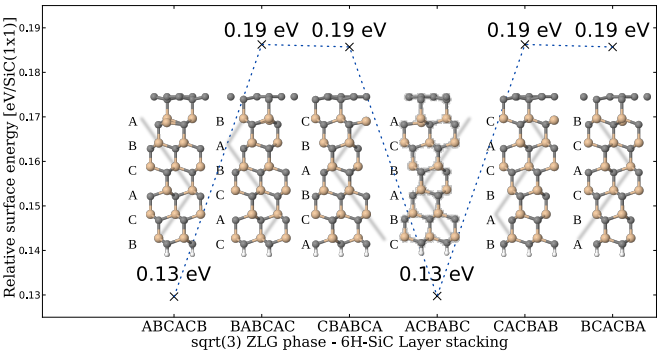

FIG. 3: The zero-layer graphene (ZLG) of the hexagonal SiC polytype (6H-SiC) using an approximated $\sqrt{3} \times \sqrt{3}$-R30° unit cell and their surface energies are shown for different SiC-bilayer stacking order calculated using PBE+vdW.

INFLUENCE OF THE POLYTYPE

To evaluate the influence of the SiC polytype on the geometry, we list the key geometry parameters in Tab. IV for the QFMLG and EMLG phase for two different polytypes, the 3C-SiC and 6H-SiC. For the QFMLG phase the interface geometries are practically identical. Likewise the interface of the EMLG phase shows polytype induced changes that are smaller than 0.04 Å. Therefore, 3C and 6H polytypes can be exchanged without qualitatively changing the result of the calculation. It should be noted that the advantage of 3C is that the number of bilayers one uses in the slab can be smaller than six.

THE ELECTRON DENSITY MAPS

We calculate the change of the electron density at the interface for the QFMLG and the EMLG phase for the 3C-SiC polytype. As shown in Tab. IV, the interface geometry hardly changes with polytype, and the same qualitative difference between the QFMLG and EMLG

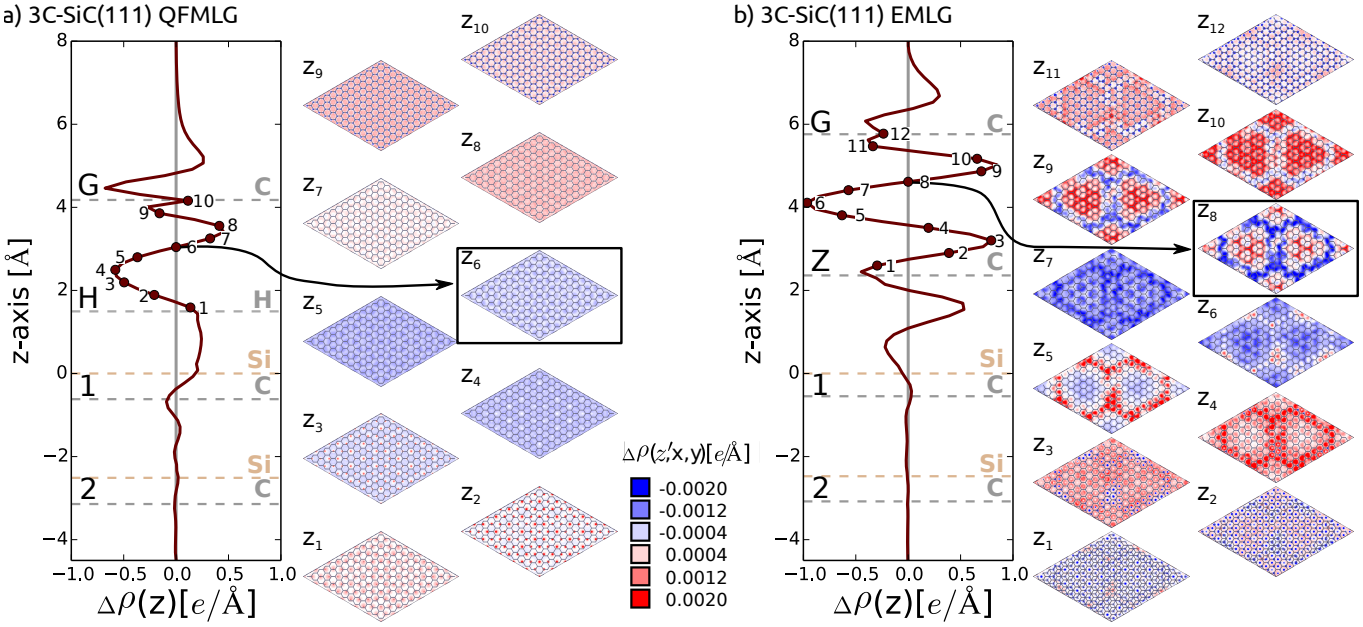

FIG. 4: The difference in the electron density ($\Delta\rho(r) = \rho_{\rm full}(r) - (\rho_{\rm G}(r) + \rho_{\rm sub}(r))$) is shown for (a) the 3C-SiC QFMLG and (b) the 3C-SiC EMLG phase. We integrated $\Delta\rho$ in the x-y-plane and plotted it along z. The position of the Si, C, H, and graphene-layer are indicated by dashed lines. We show $\Delta\rho(z_i)$ in the x-y-plane at equidistant z_i heights between the graphene layer and the substrate. In the main paper we include the electron density map at the inflection point of $\Delta\rho(z)$: z_6 for QFMLG and z_8 for EMLG.

QFMLG						
	6H-SiC			3C-SiC		
n	$D_{n,n+1}$	d_n	δ_n Si/C	$D_{n,n+1}$	d_n	δ_n Si/C
G	2.66	—	0.02	2.68	—	0.01
H	1.50	—	0.00/0.00	1.50	—	0.00/0.00
1	1.89	0.62	0.00/0.00	1.89	0.62	0.00/0.00
2	1.89	0.63	0.00/0.00	1.89	0.63	0.00/0.00
3	1.89	0.63	0.00/0.00	1.89	0.63	0.00/0.00
EMLG						
	6H-SiC			3C-SiC[6]		
n	$D_{n,n+1}$	d_n	δ_n Si/C	$D_{n,n+1}$	d_n	δ_n Si/C
G	3.40	—	0.45	3.40	—	0.41
Z	2.36	—	0.86	2.36	—	0.82
1	1.92	0.55	0.78/0.30	1.93	0.55	0.74/0.31
2	1.90	0.61	0.21/0.14	1.90	0.61	0.21/0.13
3	1.89	0.62	0.08/0.05	1.89	0.62	0.08/0.05

TABLE IV: Geometry comparison of the layer distance ($D_{n,n+1}$), the Si-C distance within a SiC bilayer (d_n) and the layer corrugation, the difference between the highest and lowest atom in the layer, (δ_n) for two different SiC polytypes, 6H-SiC(0001) and 3C-SiC(111), including both phases the QFMLG and EMLG calculated with PBE+vdW. The data for the 3C-SiC EMLG phase was taken from [6].

phases can be observed for the 6H-SiC polytype. The electron density ($\rho(r)$) of a 4-bilayer 3C-SiC slab is represented on an evenly distributed grid ($260 \times 260 \times 350$) for the full system $\rho_{\rm full}(r)$, the graphene layer alone $\rho_{\rm G}(r)$ and the substrate alone $\rho_{\rm sub}(r)$ including the H layer for the QFMLG phase and the ZLG for the EMLG phase. The electron density difference $\Delta\rho(r)$ is given by $\Delta\rho(r) = \rho_{\rm full}(r) - (\rho_{\rm G}(r) + \rho_{\rm sub}(r))$. The change in the electron density along the z-axis $\Delta\rho(z) = \int dx\, dy\, \Delta\rho(r)$ is shown in Fig. 4 (a) for the QFMLG and Fig. 4 (b) for the EMLG. Figure 4 shows $\Delta\rho(r)$ in the x-y-plane at equidistant heights of 0.3 Å at the interface region. In the main paper we include the electron density map $\Delta\rho(z_{(6,8)}, x, y)$ at the inflection point $z = z_{(6,8)}$ of $\Delta\rho(z)$. In the QFMLG all Si atoms are saturated by hydrogen resulting in small variation of the charge density within the x-y-plane (Fig. 4 (a)) independent of the chosen height. In the EMLG phase the in-plane electron density is influenced by the interplay of saturated and unsaturated Si bonds in the ZLG layer. The modulations in the charge distribution Fig. 4 (b) are visible at any chosen position z_i in the interface region.

* Electronic address: f.bocquet@fz-juelich.de

[1] D. P. Woodruff, Prog. Surf. Sci. **57**, 1 (1998).
[2] I. A. Vartanyants and M. V. Kovalchuk, Rep. Prog. Phys. **64**, 1009 (2001).
[3] D. P. Woodruff, Rep. Prog. Phys. **68**, 743 (2005).
[4] G. J. Jackson, B. C. C. Cowie, D. P. Woodruff, R. G. Jones, M. S. Kariapper, C. Fisher, A. S. Y. Chan, and M. Butterfield, Phys. Rev. Lett. **84**, 2346 (2000).
[5] P. Lauffer, K. V. Emtsev, R. Graupner, T. Seyller,

L. Ley, S. A. Reshanov, and H. B. Weber, Phys. Rev. B **77**, 155426 (2008), URL http://link.aps.org/doi/10.1103/PhysRevB.77.155426.

[6] L. Nemec, V. Blum, P. Rinke, and M. Scheffler, Phys. Rev. Lett. **111**, 065502 (2013).

[7] V. Blum, R. Gehrke, F. Hanke, P. Havu, V. Havu, X. Ren, K. Reuter, and M. Scheffler, Comp. Phys. Comm. **180**, 2175 (2009).

[8] J. P. Perdew and Y. Wang, Phys. Rev. B **45**, 13244 (1992).

[9] J. P. Perdew, K. Burke, and M. Ernzerhof, Phys. Rev. Lett. **78**, 1396 (1997).

[10] A. V. Krukau, O. A. Vydrov, A. F. Izmaylov, and G. E. Scuseria, J. Chem. Phys. **125**, 224106 (2006).

[11] A. Tkatchenko and M. Scheffler, Phys. Rev. Lett. **102**, 073005 (2009).

[12] A. Tkatchenko, R. A. DiStasio, R. Car, and M. Scheffler, Phys. Rev. Lett. **108**, 236402 (2012).

[13] A. Tkatchenko, A. Ambrosetti, and R. A. DiStasio, J. Chem. Phys. **138**, 074106 (2013).

[14] A. Ambrosetti, A. M. Reilly, R. A. DiStasio, and A. Tkatchenko, J. Chem. Phys. **140**, 18A508 (2014).